JPE 6-1-7

Maximum Power Point Tracking Control Scheme for Grid Connected Variable Speed Wind Driven Self-Excited Induction Generator

Fayez F. M. El-Sousy†, Mohamed Orabi* and Hatem Godah**

†**Electronics Research Institute (ERI), Power Electronics & Energy Conversion Department, Dokki, Cairo, Egypt
*Electrical Power and Machines Department, Faculty of Engineering, South Valley University, Aswan, Egypt

ABSTRACT

This paper proposes a wind energy conversion system connected to a grid using a self-excited induction generator (SEIG) based on the maximum power point tracking (MPPT) control scheme. The induction generator (IG) is controlled by the MPPT below the base speed and the maximum energy can be captured from the wind turbine. Therefore, the stator currents of the IG are optimally controlled using the indirect field orientation control (IFOC) according to the generator speed in order to maximize the generated power from the wind turbine. The SEIG feeds a (CRPWM) converter which regulates the DC-link voltage at a constant value where the speed of the IG is varied. Based on the IG d-q axes dynamic model in the synchronous reference frame at field orientation, high-performance synchronous current controllers with satisfactory performance are designed and analyzed. Utilizing these current controllers and IFOC, a fast dynamic response and low current harmonic distortion are attained. The regulated DC-link voltage feeds a grid connected CRPWM inverter. By using the virtual flux orientation control and the synchronous frame current regulators for the grid connected CRPWM inverter, a fast current response, low harmonic distortion and unity power factor are achieved. The complete system has been simulated with different wind velocities. The simulation results are presented to illustrate the effectiveness of the proposed MPPT control scheme for a wind energy system. In the simulation results, the d-q axes current controllers and DC-link voltage controller give prominent dynamic response in command tracking and load regulation characteristics.

Keywords: SEIG, IFOC, Wind Energy, CRPWM Converter, DC-Link Voltage Control, CRPWM Inverter

1. Introduction

Recently, the wind generation system is attracting attention as a clean and safe renewable power source. Induction machines have many advantageous characteristics such as high robustness, reliability and low cost. Therefore, induction machines are used in high-performance applications, which require independent torque and flux control. The induction machines may be used as a motor or a generator. Self-excited induction generators (SEIG) are good candidates for wind-power electricity generation especially in remote areas, because they do not need an external power supplies to produce the excitation magnetic fields[1-3]. The excitation can be provided by a capacitor bank connected to the stator

Manuscript received August 6, 2004; revised Nov. 21, 2005
†Corresponding Author: fayez@eri.sci.eg
Tel: +202-310554, Fax: +202-3351631, ERI
**Electronics Research Institute (ERI)
*South Valley University

windings of the induction generator. Magnetizing inductance is the main factor for voltage build-up of the IG. The minimum and maximum values of capacitance required for self-excitation have been analyzed previously [4-7].

The three phase current regulated pulse-width modulation (CRPWM) AC/DC/AC converters have been increasingly used for wind energy system applications. Their attractive features include: regulated DC-link voltage, low harmonic distortion of the induction generator currents and controllable power factor and efficiency [8-9]. The current regulation of a SEIG in the synchronous frame has the advantages of fast dynamic current response, good accuracy, constant switching frequency and less sensitivity to parameter variations.

In wind generation systems, a variable speed generation system is more attractive than a fixed speed one because of the improvement in the wind energy production. In a variable speed system, wind turbine can be operated to produce its maximum power at every wind speed by adjusting the shaft speed optimally. In order to achieve the maximum power point tracking (MPPT) control, some control schemes have been studied. For example, a search-based or perturbation-based strategy [10,11], a fuzzy-logic based control [12,13], a wind speed-estimation-based algorithm [14] has been applied.

In this paper, a variable speed high performance generation system using a SIEG is studied. The requirements of high dynamic performance is gained utilizing filed-oriented control (FOC) in which the dynamic model of the induction generator is simplified and decoupled. The FOC strategy studied in this context was developed by Hass and Blashke in Germany some thirty years ago. This technique improves the performance of the induction generator to a level comparable to that of a separately excited DC generator. Therefore, the FOC of an induction generator system permits a high performance dynamic response using decoupled torque and flux control. The FOC strategy can be classified into two types, the direct filed orientation control (DFOC) and indirect filed orientation control (IFOC). The IFOC strategy is simpler than the DFOC strategy. The orientation technique may be done for rotor or stator and/or air-gap flux. The rotor flux orientation is the best one because there is a linear relation between the electromagnetic torque and the stator torque current of the induction generator. Some control schemes have been studied using DFOC [15,16] and IFOC with stator flux orientation [17].

The IFOC of the SEIG for the WECS is composed of a dynamic model of the wind turbine, a dynamic model of the IG in the arbitrary and synchronously rotating reference frames, a dynamic model of the IFOC technique (decoupling controller), d-q axes current controllers, a voltage controller, coordinate transformations, a space-vector PWM (SVPWM) and AC/DC/AC CRPWM converters as shown in Fig. 1.

In the proposed wind generation system, the control scheme is based on the MPPT technique. The IFOC technique with the rotor flux of a SEIG is used for controlling the CRPWM converter while the grid connected CRPWM inverter is controlled utilizing the vector control technique. The current vector of the SEIG is suitably controlled according to the IG speed in order to optimize the wind turbine operation for various wind speeds. The IFOC of the SEIG allows for control of the d-q stator currents. So, the output voltage of the CRPWM converter can be regulated and we can maximize the efficiency. In the proposed control scheme with the IFOC of the SEIG, a dynamic model of the induction generator in d-q axes arbitrary reference frame is carried out. At field orientation control (FOC), $\lambda_{qr}=0$, $d\lambda_{qr}/dt=0$, $d\lambda_{dr}/dt=0$ and $\omega_m=\omega_e$, the IFOC is derived in the synchronous reference frame. Based on the transfer function of the IG at FOC, the proportional plus integral (PI) current controllers in the d-q axes are designed and analyzed to meet the time domain specifications: minimum overshot, minimum settling time and minimum steady-state error. After that, a PI voltage controller is designed to accomplish the specifications of the voltage control loop based on the dynamic of the DC-link and the SEIG. Also, this paper studies the design and control of the grid connected CRPWM inverter with the MPPT algorithm and unity power factor. Similarly, by applying the vector control technique to the grid connected CRPWM inverter, we can deduce the transfer function of the inverter with the grid at virtual-flux orientation control (VFOC) and the design of the d-q axes current controllers are accomplished. To verify the design of the controllers and

system performance, the WECS is simulated starting with the wind turbine, the SEIG and then the AC/DC/AC CRPWM converter. The dynamic performance of the WECS has been studied under different wind velocities and MPPT. The simulation results are provided to demonstrate the effectiveness of the proposed control scheme.

2. System Description

2.1 Composition of Wind Generator System

The wind power generation system studied in this paper is shown in Fig. 1. The wind turbine is coupled to the shaft of a self-excited induction generator (IG) through a gear box. The IG is connected to a CRPWM voltage source converter with current and voltage regulation utilizing IFOC control of the induction generator. The generated DC power is transferred to the utility grid through a CRPWM voltage source inverter using a vector control technique.

2.2 Wind Turbine Characteristics

Wind turbines are characterized by the non-dimensional curve of the performance coefficient as a function of tip-speed ratio λ. The mechanical input power P_m of a fixed-pitch wind turbine as a function of the effective wind velocity v_w through the blades, the air density, ρ, the blades' radius R and the power coefficient C_p is given by:

$$P_m = \frac{1}{2}\rho R^2 v_w^3 C_p(\lambda) \tag{1}$$

Considering the rotational speed of the wind turbine ω_t and the torque coefficient $C_t(\lambda)$, the wind turbine mechanical torque is given by:

$$T_m = \frac{1}{2}\rho R^3 v_w^2 C_t(\lambda) \tag{2}$$

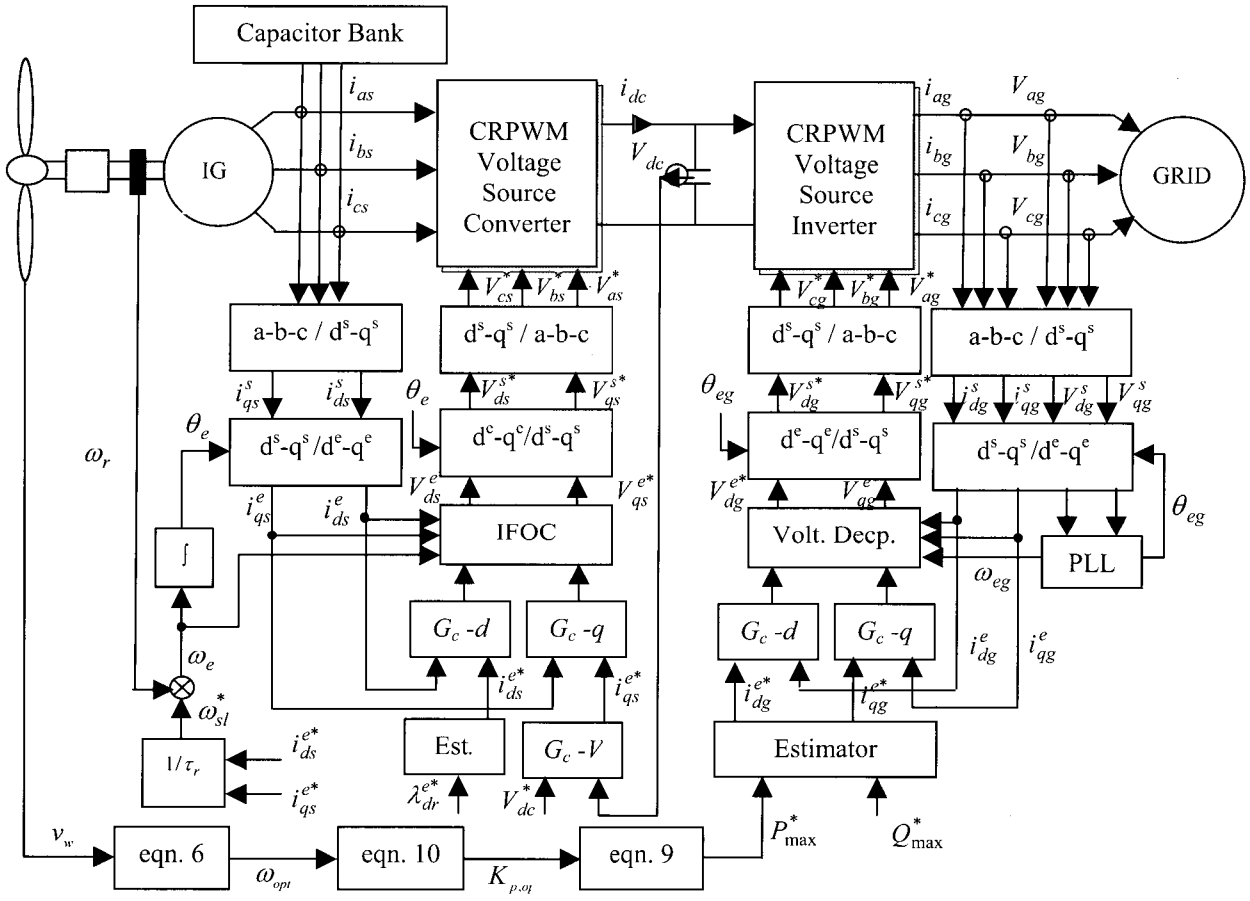

Fig. 1 Self-excited induction generator wind energy conversion system

$$C_p(\lambda) = \lambda C_t(\lambda) \tag{3}$$

Where,

$$\lambda = \frac{\omega_t R}{v_w} \tag{4}$$

The turbine power coefficient $C_p(\lambda)$ is a function of the tip-speed ratio of the blades if the pitch angle of the blade is constant. The turbine power coefficient is represented by various approximation expressions. In this paper, $C_p(\lambda)$ is approximated using a fifth-order polynomial curve fit given by the following equation and it is shown in Fig. 2.

$$C_p(\lambda) = 0.0201 - 0.1022\lambda + 0.0537\lambda^2 - 0.0063\lambda^3 + 0.000284\lambda^4 - 0.0000045\lambda^5 \tag{5}$$

The power and torque versus speed curves of the wind turbine can be calculated by (1)-(5) at various wind speeds. The parameters of the wind turbine used in this paper are listed in Table 1.

2.3 Maximum Power Point Tracking (MPPT) Control

The optimum rotational speed ω_{opt} for maximum mechanical power of the wind turbine is given by:

$$\omega_{opt} = \frac{\lambda_{opt}}{R} v_w \tag{6}$$

The maximum mechanical power $P_{m;max}$ is obtained from the wind energy equation as follows:

$$P_{m,\max} = K_{p,\max} v_w^3 \tag{7}$$

Where,

$$K_{p,\max} = \frac{1}{2} \rho R^2 C_{p,\max} \tag{8}$$

Substituting from (6) into (7), the maximum power curve versus generator speed can be drawn at various wind speeds and it is shown in Fig. 3. In this paper, the maximum mechanical power of the wind turbine is given by:

$$P_{m,\max} = K_{p,opt} \omega_{opt}^3 \tag{9}$$

where,

$$K_{p,opt} = \frac{1}{2} \rho C_{p,\max} \frac{R^5}{\lambda_{opt}^3} \tag{10}$$

Thus, the corresponding optimal torque is:

$$T_{opt} = K_{p,opt} \omega_{opt}^2 \tag{11}$$

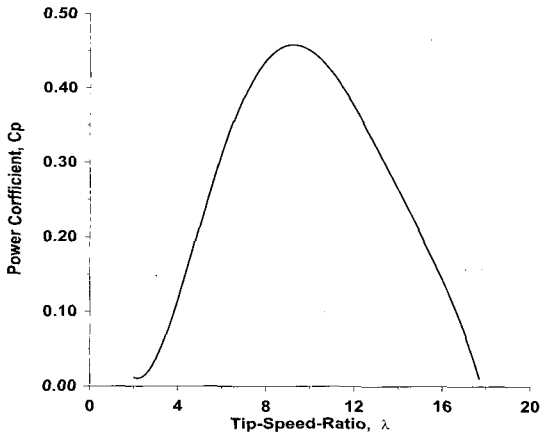

Fig. 2 Power coefficient versus tip-speed-ratio

Fig. 3 shows the optimum operating point for obtaining the maximum mechanical power versus the speed curve at various wind speeds. These optimum points correspond to the condition in which the power coefficient *Cp* becomes a maximum. From Fig. 2, the maximum value of the power coefficient, $C_{p\text{-}max}$ equals 0.46 at the maximum tip speed ratio λ_{max}, of about 9.2. When the generator speed is always controlled at the optimum speed given in (6), the tip-speed ratio remains the optimum value and the maximum power point tracking (MPPT) control can be achieved. In this case, information on wind speed is required. At any wind speed, we can calculate the optimum rotational speed of the generator from (6), and then the maximum mechanical power is calculated from (9). The maximum power is used as the power reference to the grid connected current regulated pulse width modulation (CRPWM) inverter.

3. Mathematical Modeling of the SEIG

The dynamic model of the induction generator is

helpful for analyzing all its characteristics. The induction machine used as the SEIG is a three-phase squirrel-cage machine. The machine parameters are listed on Table 2. In this paper, the d-q model in the arbitrary reference frame is used because it provides a complete solution for dynamics analysis and control. The voltage equation of the d-q model is based on the stator currents and rotor fluxes are given as:

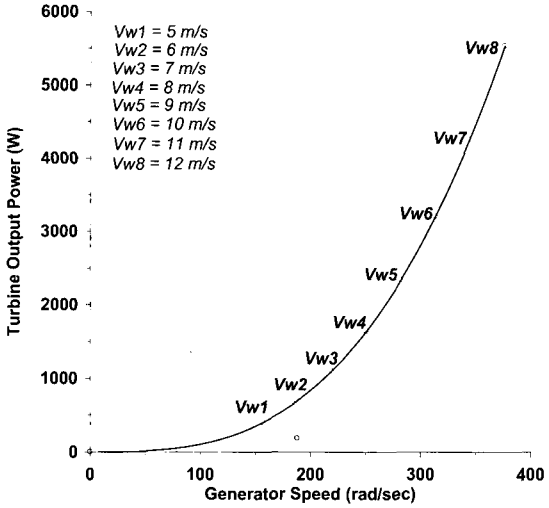

Fig. 3 Maximum mechanical power of the wind turbine at various wind speeds

$$\begin{bmatrix}0\\0\\0\\0\end{bmatrix}=\begin{bmatrix}(R_s+L_s\sigma p) & \omega L_s\sigma & \frac{L_m}{L_r}p & \frac{L_m}{L_r}\omega\\ -\omega L_s\sigma & (R_s+L_s\sigma p) & -\frac{L_m}{L_r}\omega & \frac{L_m}{L_r}p\\ -\frac{L_m}{L_r}R_r & 0 & \left(\frac{R_r}{L_r}+\mathrm{p}\right) & (\omega-\omega_r)\\ 0 & -\frac{L_m}{L_r}R_r & -(\omega-\omega_r) & \left(\frac{R_r}{L_r}+\mathrm{p}\right)\end{bmatrix}\begin{bmatrix}i_{qs}\\ i_{ds}\\ \lambda_{qr}\\ \lambda_{dr}\end{bmatrix}+\begin{bmatrix}v_{qs}\\ v_{ds}\\ v_{qr}\\ v_{dr}\end{bmatrix} \tag{12}$$

$$V_{qs}=\frac{1}{C}\int i_{qs}dt+V_{cq}\Big|_{t=0} \tag{13-a}$$

$$V_{ds}=\frac{1}{C}\int i_{ds}dt+V_{cd}\Big|_{t=0} \tag{13-b}$$

The electromagnetic torque is given by:

$$T_e=-\frac{3}{2}\frac{P}{2}\frac{L_m}{L_r}\left(\lambda_{dr}i_{qs}-\lambda_{qr}i_{ds}\right) \tag{14}$$

Where, V_{qs}, V_{ds}, i_{qs}, and i_{ds} are the stator voltages and currents, respectively. v_{qr} and v_{dr} are the rotor voltages. λ_{qr} and λ_{dr} are the rotor fluxes. R_s, L_s, R_r and L_r are the resistance and the self inductance of the stator and the rotor, respectively. L_m is the mutual inductance. The mathematical equation that relates the wind turbine output torque with the electromagnetic torque of the induction generator is given by:

$$T_m=J\frac{d}{dt}\omega_m+\beta\omega_m+T_e \tag{15}$$

$$\frac{d}{dt}\begin{bmatrix}i_{qs}\\ i_{ds}\\ \lambda_{qr}\\ \lambda_{dr}\end{bmatrix}=\frac{1}{\sigma L_s L_r}\begin{bmatrix}-(R_s L_r+R_s\frac{L_m^2}{L_r}) & -\sigma L_s L_r\omega & \frac{L_m}{L_r}R_r & -L_m\omega_r\\ \sigma L_s L_r\omega & -(R_s L_r+R_s\frac{L_m^2}{L_r}) & L_m\omega_r & \frac{L_m}{L_r}R_r\\ \sigma L_s L_m R_r & 0 & \sigma L_s L_r R_r & -\sigma L_s L_r(\omega-\omega_r)\\ 0 & \sigma L_s L_m R_r & \sigma L_s L_r(\omega-\omega_r) & \sigma L_s L_r R_r\end{bmatrix}\begin{bmatrix}i_{qs}\\ i_{ds}\\ \lambda_{qr}\\ \lambda_{dr}\end{bmatrix}+\frac{1}{\sigma L_s L_r}\begin{bmatrix}L_m v_{qr}-L_r v_{qs}\\ L_m v_{dr}-L_r v_{ds}\\ -\sigma L_s L_r v_{qr}\\ -\sigma L_s L_r v_{dr}\end{bmatrix} \tag{16}$$

$$\frac{d}{dt}\omega_m=\frac{1}{J}T_m-\frac{\beta}{J}\omega_m-\frac{1}{J}T_e \tag{17}$$

ω_m, J and β are the mechanical angular speeds of the wind turbine, the effective inertia of the wind turbine, the induction generator and the friction coefficient,

respectively. From (12)-(15), the state equations of the SEIG and turbine can be accomplished as in (16) and (17).

4. IFOC of the Induction Generator

The IFOC dynamics for the induction machine (torque, slip angular frequency and voltage commands) can be derived from (12)-(14), respectively at λ_{qr}=0, $d\lambda_{qr}/dt$=0, $d\lambda_{dr}/dt$=0, and $\omega_m=\omega_e$. The torque equation and slip angular frequency for rotor field orientation are given in (18)-(19) while the voltage commands of the IFOC are given in (20)-(21):

$$T_e = \frac{3}{2}\cdot\frac{P}{2}\cdot\frac{L_m^2}{L_r} i_{ds}^{e*} i_{qs}^{e*} \tag{18}$$

$$\omega_{sl} = \frac{1}{\tau_r}\cdot\frac{i_{qs}^{e*}}{i_{ds}^{e*}} \tag{19}$$

$$\begin{bmatrix} V_{qs}^{e*} \\ V_{ds}^{e*} \end{bmatrix} = \begin{bmatrix} e_{qs}^{e} \\ e_{ds}^{e} \end{bmatrix} - \begin{bmatrix} R_s + L_s\sigma\frac{d}{dt} & \omega_e L_s\sigma \\ -\omega_e L_s\sigma & R_s + L_s\sigma\frac{d}{dt} \end{bmatrix} \begin{bmatrix} i_{qs}^{e} \\ i_{ds}^{e} \end{bmatrix} \tag{20}$$

$$\begin{bmatrix} e_{qs}^{e} \\ e_{ds}^{e} \end{bmatrix} = \begin{bmatrix} \omega_e \lambda_{dr}^{e} \frac{L_m}{L_r} \\ 0 \end{bmatrix} \tag{21}$$

Where, e^e_{qs} and e^e_{ds} are the back EMFs of the machine. T_e, τ_r, ω_{sl}, and ω_e are the electromagnetic torque, the rotor time constant, the slip angular frequency, and the angular frequency of the synchronous reference frame, respectively.

5. Dynamic Model of the IFOC CRPWM Voltage Source Converter

The block diagram of the IFOC PWM voltage source converter is shown in Fig. 4. It is well known that the IFOC of induction machines allows for the independent control of two input variables, stator quadrature axis current i^e_{qs} and stator direct axis current i^e_{ds}. This suggests that it is possible to control the output voltage and power factor and/or efficiency by controlling the two components of the stator currents.

The dynamic equations of the CRPWM converter in the synchronous reference frame are based on the IFOC dynamics of the IG. Therefore, the dynamics of the CRPWM converter is given by (22)-(23).

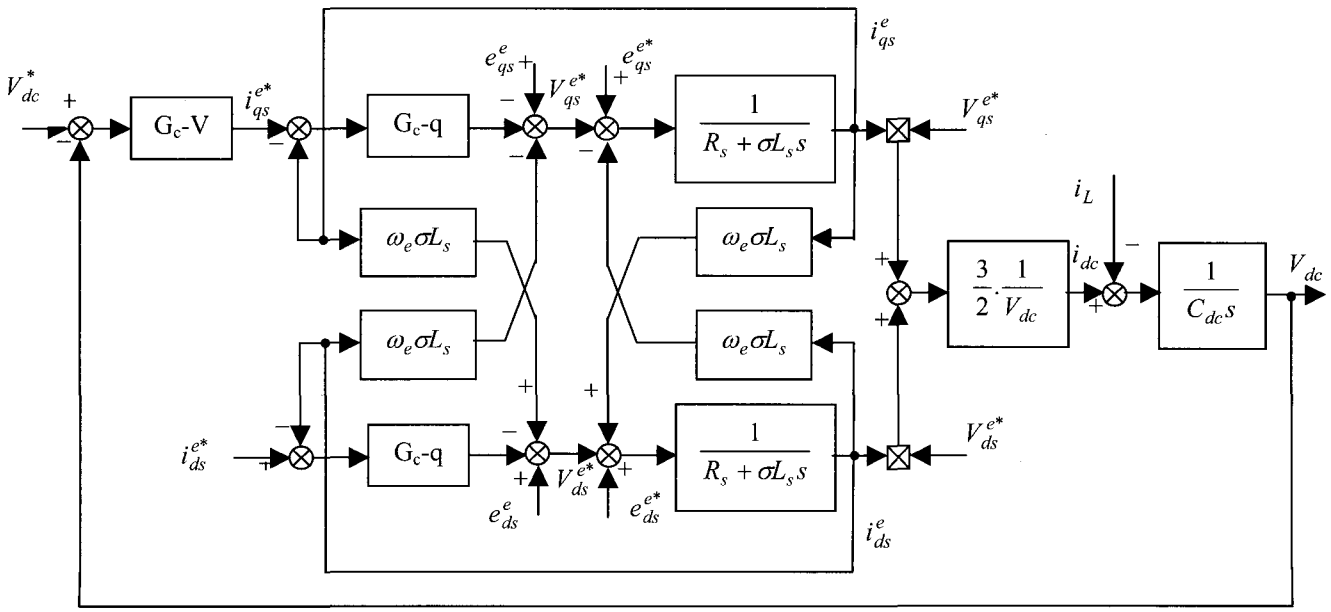

Fig. 4 Block Diagram of the IFOC CRPWM voltage source converter

The dynamic equations of the CRPWM converter in the synchronous reference frame are based on the IFOC dynamics of the IG. Therefore, the dynamics of the CRPWM converter is given by (22)-(23).

$$e_{qs}^{e} - V_{qs}^{ec} = (R_s + L_s \sigma p) i_{qs}^{ec} + \omega_e L_s \sigma i_{ds}^{ec} \tag{22}$$

$$e_{qs}^{e} - V_{qs}^{ec} = (R_s + L_s \sigma p) i_{ds}^{ec} - \omega_e L_s \sigma i_{qs}^{ec} \tag{23}$$

By considering the converter as an ideal current regulated source, the energy is transferred between the induction generator and the dc-link. As a consequence, the instantaneous power of both the converter's ac-side and dc-side is the same.

$$V_{dc} i_{dc} = \frac{3}{2}\left(V_{qs}^{e} i_{qs}^{e} + V_{ds}^{e} i_{ds}^{e}\right) \tag{24}$$

From this equation, we can deduce the relation between the dc-link current i_{dc} and the q-axis current i^{e}_{qs} as follows.

$$i_{qs}^{e} = \frac{2}{3}\left(\frac{V_{dc}}{V_{qs}^{e}} i_{dc}\right) - \frac{V_{ds}^{e}}{V_{qs}^{e}} i_{ds}^{e} \tag{25}$$

At FOC V^{e}_{ds}=0, therefore, there is a direct relation between the DC-link current and the q-axis current of the IG.

$$i_{qs}^{e} = \frac{2}{3}\frac{V_{dc}}{V_{qs}^{e}} i_{dc} \tag{26}$$

The dynamics of the dc-link is given by:

$$C_{dc}\frac{d}{dt}V_{dc} + i_L = i_{dc} \tag{27}$$

$$i_{dc} = \frac{3}{2}\frac{V_{qs}^{e}}{V_{dc}} i_{qs}^{e} \tag{28}$$

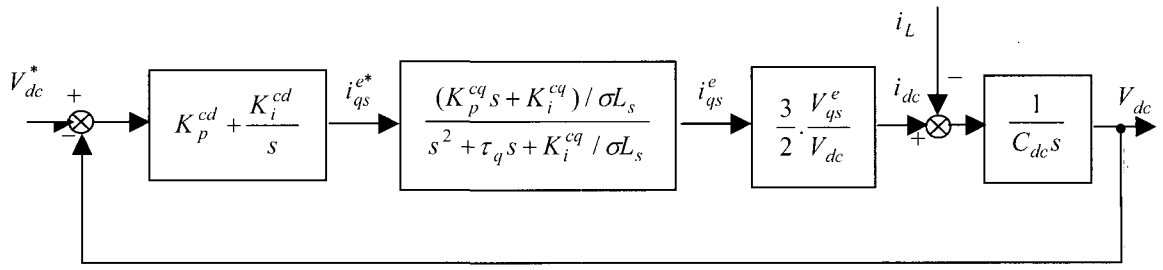

Fig. 5 Block diagram of the CRPWM converter voltage control loop

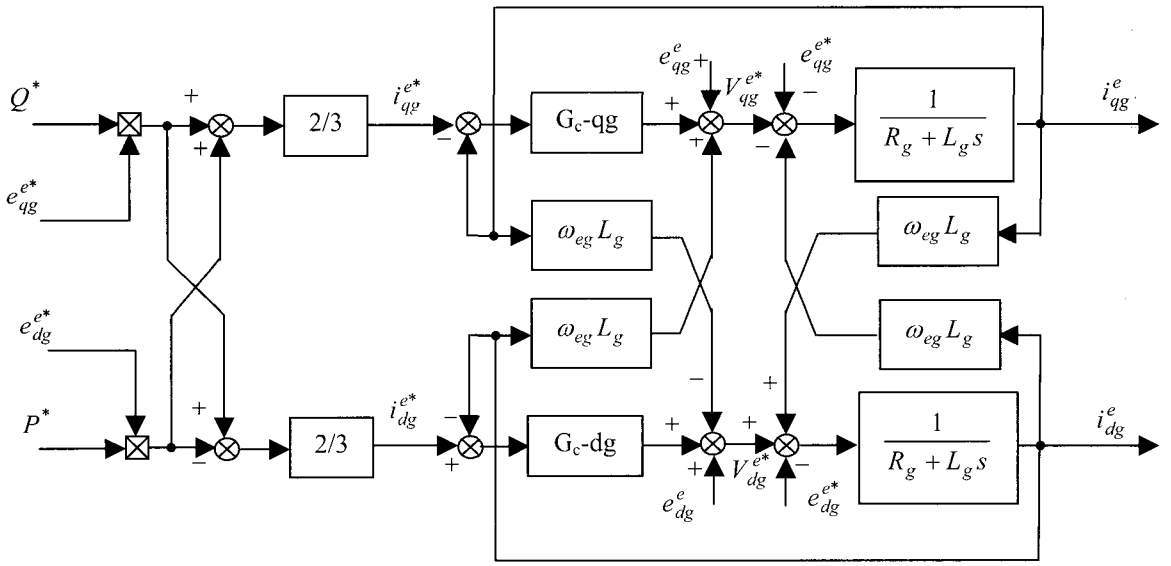

Fig. 6 Block Diagram of the vector controlled CRPWM voltage source converter

Where, C_{dc} is the DC-link capacitor, i_L is the load current and i_{dc} is the DC-link current. The state equation of the CRPWM converter and DC-link are derived from (22), (23) and (27) as follows.

$$\frac{d}{dt}\begin{bmatrix} i_{qs}^{ec} \\ i_{ds}^{ec} \end{bmatrix} = \frac{1}{\sigma L_s}\begin{bmatrix} -R_s & \omega_e L_s \sigma \\ -\omega_e L_s \sigma & R_s \end{bmatrix}\begin{bmatrix} i_{qs}^{ec} \\ i_{ds}^{ec} \end{bmatrix} + \begin{bmatrix} e_{qs}^{e} - V_{qs}^{ec} \\ e_{ds}^{e} - V_{ds}^{ec} \end{bmatrix} \tag{29}$$

$$\frac{d}{dt}V_{dc} = \frac{1}{C_{dc}}\begin{bmatrix} \frac{3}{2}\frac{V_{qs}^{ec}}{V_{dc}} & -1 \end{bmatrix}\begin{bmatrix} i_{qs}^{ec} \\ i_L \end{bmatrix} \tag{30}$$

6. Design of the CRPWM Converter Controllers

In this section, quantitative design procedures of the d-q axes currents and voltage controllers for the CRPWM converter are described. These controllers are designed based on the IG dynamic model at IFOC and DC-link dynamic model respectively.

6.1 The d-q Axes Current Controllers Design

This section considers the design procedure of the current controllers based on the voltage equations of the SEIG at IFOC. A systematic design procedure for the proportional plus integral (PI) current controllers capable of satisfying the desired specifications is given. From the block diagram shown in Fig. 4, a back EMF estimator is adopted to q-axis current loop for voltage feed-forward control. By exercising the decoupling control, the model including the converter and the induction generator can be simplified and the closed loop transfer function is given by:

$$\frac{i_{qs}^{e}}{i_{qs}^{e*}} = \frac{(K_p^{cq} s + K_i^{cq})/\sigma L_s}{s^2 + s(R_s + T_q + K_p^{cq})/\sigma L_s + K_i^{cq}/\sigma L_s} \cong \frac{\omega_n^2}{s^2 + 2\zeta\omega_n s + \omega_n^2} \tag{31}$$

Where,

$$T_q = \left(\frac{\omega_{sl} + \omega_r}{\tau_r \omega_{sl}}\right)\left(\sigma L_s + \frac{L_m^2}{L_r}\right) \tag{32}$$

From (31), the controller parameters can be expressed as:

$$\begin{aligned} K_i^{cq} &= \omega_n^2 \sigma L_s \\ K_p^{cq} &= (2\zeta\omega_n \sigma L_s - R_s - T_q) \end{aligned} \tag{33}$$

Similarly, the closed loop transfer function of the d-axis current loop is given by:

$$\frac{i_{ds}^{e}}{i_{ds}^{e*}} = \frac{(K_p^{cd} s + K_i^{cd})/\sigma L_s}{s^2 + s(R_s + T_d + K_p^{cd})/\sigma L_s + K_i^{cd}/\sigma L_s} \cong \frac{\omega_n^2}{s^2 + 2\zeta\omega_n s + \omega_n^2} \tag{34}$$

Where,

$$T_d = (\omega_{sl} + \omega_r)\omega_{sl}\tau_s \sigma L_s \tag{35}$$

From (34), the controller parameters can be expressed as:

$$\begin{aligned} K_i^{cd} &= \omega_n^2 \sigma L_s \\ K_p^{cd} &= (2\zeta\omega_n \sigma L_s - R_s + T_d) \end{aligned} \tag{36}$$

Where, ζ is the damping ratio and ω_n is the natural frequency of the current loop.

6.2 Voltage Controller Design

The main task of the induction generator is to regulate the dc-link voltage. According to the analysis accomplished in the previous section, the q-axis stator current of the induction generator is selected as the variable to be changed to regulate the dc-link voltage. The voltage control is carried out through a voltage control loop using a PI controller. The block diagram of the voltage control loop is shown in Fig. 5. The closed loop transfer function of the voltage control loop is given by:

$$\left.\frac{V_{dc}(s)}{V_{dc}^{*}(s)}\right|_{i_L=0} = \frac{(K_{dc}/\sigma L_s C_{dc})(a_2 s^2 + a_1 s + a_o)}{s^4 + b_3 s^3 + b_2 s^2 + b_1 s + b_o} \cong \frac{\omega_n^4}{s^4 + 2.1\omega_n s^3 + 3.4\omega_n^2 s^2 + 2.7\omega_n^3 s + \omega_n^4} \tag{37}$$

From (37), the controller parameters are:

$$K_i^v = \frac{C_{dc}}{K_{dc}} \frac{\sigma L_s}{K_i^{cq}} \omega_n^4$$
$$K_p^v = \frac{C_{dc}}{K_{dc} K_p^{cq}} (3.4\sigma\omega_n^2 - K_i^{cq}) \quad (38)$$

7. Dynamic Model of the Grid Connected CRPWM Voltage Source Inverter

The grid connected CRPWM inverter is used to inject the generated power into the grid. By using vector control techniques, the currents of the CRPWM inverter are controlled with very high bandwidth. The orientation of the reference frame is done along the supply voltage vector to obtain the decoupled control of the active and reactive power. Usually, the reactive power component current is set to zero for unity power factor operation. The primary aim of this control scheme is to modulate the inverter to regulate the magnitude and the phase angle of the grid supply current, so that the active and reactive power entering the network can be controlled. The procedure for modeling the CRPWM inverter is based on the VFOC technique. For modeling and control design, three phase variables in the stationary frame can be transferred to the synchronous frame. The differential equation of the PWM inverter can be expressed as follows:

$$\begin{bmatrix} V_{qg}^{e*} \\ V_{dg}^{e*} \end{bmatrix} = \begin{bmatrix} e_{qg}^{e} \\ e_{dg}^{e} \end{bmatrix} + \begin{bmatrix} R_g + L_g p & \omega_{eg} L_g \\ -\omega_{eg} L_g & R_g + L_g p \end{bmatrix} \begin{bmatrix} i_{qg}^{e} \\ i_{dg}^{e} \end{bmatrix} \quad (39)$$

For balanced three-phase system,

$$\begin{bmatrix} e_{qs}^{e} \\ e_{ds}^{e} \end{bmatrix} = \begin{bmatrix} 0 \\ V_{mg} \end{bmatrix} \quad (40)$$

The d-q current commands of the inverter can be expressed as:

$$\begin{bmatrix} i_{qg}^{e*} \\ i_{dg}^{e*} \end{bmatrix} = \frac{2}{3} \begin{bmatrix} e_{qg}^{e*} & e_{dg}^{e*} \\ e_{dg}^{e*} & -e_{qg}^{e*} \end{bmatrix} \begin{bmatrix} Q^* \\ P^* \end{bmatrix} \quad (41)$$

Where, P^* and Q^* denote the required input active and reactive powers of the inverter that come from the wind energy system. To achieve the unity power factor operation, Q^* must be zero. From (40) and (41),

$$\begin{bmatrix} i_{qg}^{e*} \\ i_{dg}^{e*} \end{bmatrix} = \begin{bmatrix} 0 \\ \frac{2}{3} \frac{P^*}{V_{mg}} \end{bmatrix} \quad (42)$$

From (42), it is obvious that the current command of the q-axis must be zero for unity power factor operation and the current command of the d-axis can be evaluated from the required input active power. It is seen from (40) that coupling terms exist in the d-q current control loops. The d-q voltage decouplers are designed to decouple the current control loops. Suitable feed-forward control components of grid voltages are also added to speed up current responses. The d-q current control loops of the PWM inverter in the proposed system are shown in Fig. 6.

8. Design of the CRPWM Inverter Controllers

The d-q voltage commands are assumed to be not saturated for linear operation of the PWM modulation with the d-q current control loops being fully decoupled. The current control loops shown in Fig. 7 can be simplified. The closed transfer function is given by:

$$\frac{i_{qg}^{e}}{i_{qg}^{e*}} = \frac{(K_p^{qg} s + K_i^{qg}) / L_g}{s^2 + s(R_g + gK_p^{qg}) / L_g + K_i^{qg} / L_g} \cong \frac{\omega_n^2}{s^2 + 2\zeta\omega_n s + \omega_n^2} \quad (43)$$

From (43), the PI current controller parameters are determined as follows:

$$K_i^{qg} = \omega_n^2 L_g$$
$$K_p^{qg} = (2\zeta\omega_n L_g - R_g) \quad (44)$$

Similarly, the closed loop transfer function of the q-axis current loop is deduced as:

$$\frac{i_{dg}^{e}}{i_{dg}^{e*}} = \frac{(K_p^{dg} s + K_i^{dg}) / L_g}{s^2 + s(R_g + gK_p^{dg}) / L_g + K_i^{dg} / L_g} \cong \frac{\omega_n^2}{s^2 + 2\zeta\omega_n s + \omega_n^2} \quad (45)$$

From (45), the PI current controller parameters are determined as follows:

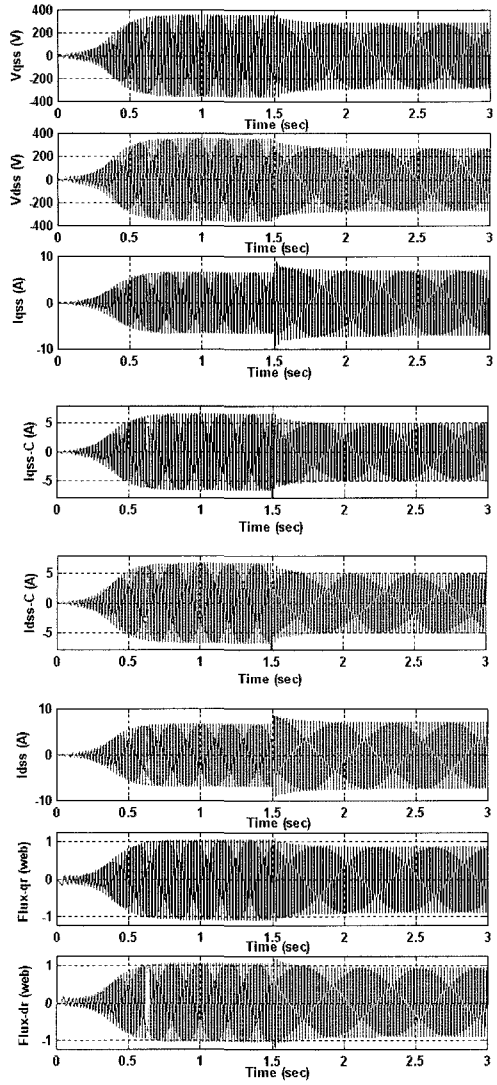

Fig. 7 Self excitation dynamic performance of the induction generator at C=55 μF continue

$$K_i^{dg} = \omega_n^2 L_g$$
$$K_p^{dg} = (2\zeta\omega_n L_g - R_g) \quad (46)$$

9. Simulation Results

This section presents a computer simulation of the proposed control scheme. The SEIG wind turbine energy conversion system interconnected to the grid simulation is carried out using a MATLAB/SIMULINK package. The dynamic performance of the whole system for different operating conditions is studied.

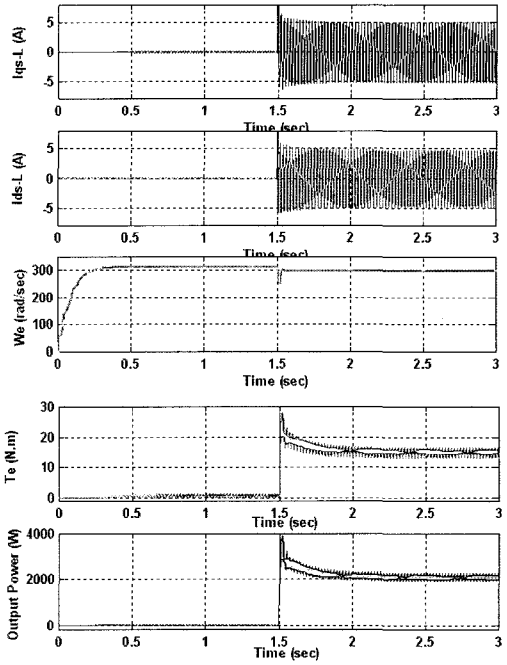

Fig. 7 Self excitation dynamic performance of the induction generator at C=55 μF

9.1 Dynamic Performance of SEIG

MATLAB/SIMULINK simulation software was used to predict the no-load voltage of a three-phase induction generator rotating at rated speed with an appropriate capacitor connected at the stator terminals. The wind turbine is used as the prime-mover for the induction generator. Once the voltage reaches its steady-state value, load is connected across the generator. Fig. 7 shows the self-excitation performance of the induction generator. The dynamic performance includes the d-q stator voltage, d-q stator currents, d-q rotor fluxes, d-q capacitor currents, frequency, torque and power at no load and loading conditions.

9.2 Dynamic Performance of IFOC SEIG Feeding CRPWM Converter

The dynamic performances of the proposed IFOC technique of the SEIG feeding CRPWM converter for start-up, wind speed variation and load variation are shown in Figs. 8-11. The IFOC variables at no-load are illustrated in Fig. 8. The results confirm the strategy of the IFOC for the SEIG. At field orientation, the stator voltage is aligned to the q-axis and the d-axis voltage is

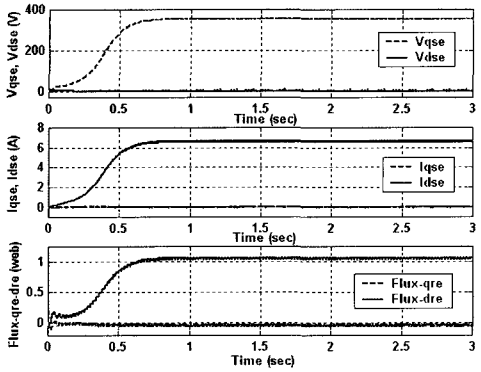

Fig. 8 IFOC variables at no-load

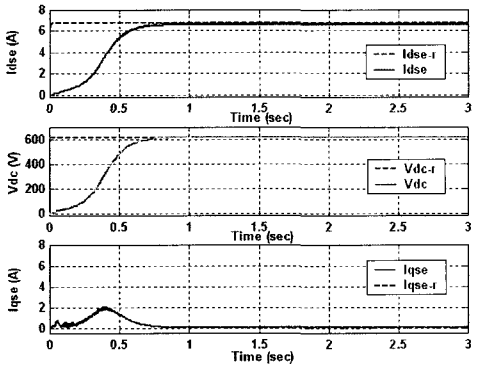

Fig. 9 Dynamic performance of the CRPWM converter at no-load

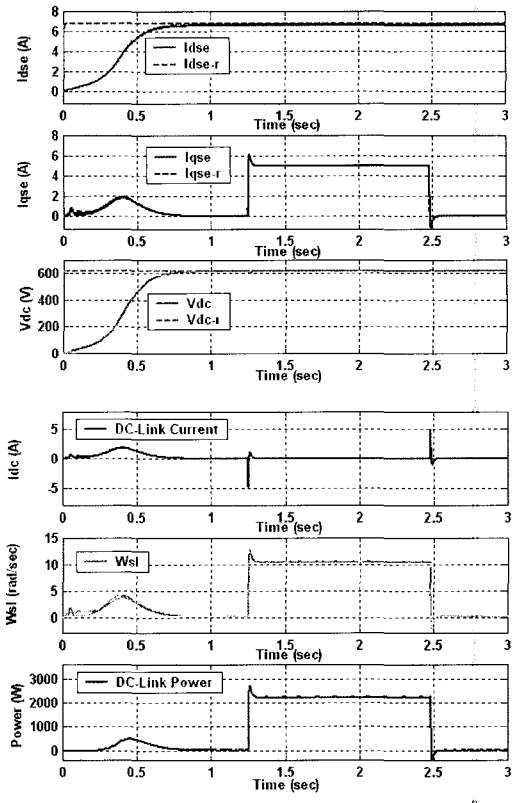

Fig. 10 Dynamic performance of the CRPWM converter at loading condition continue

maintained at zero. Also, the rotor flux is aligned to the d-axis while the q-axis rotor flux is maintained at zero. The d-q axes current control and DC-link voltage control are given in Fig. 9 at no-load. The CRPWM converter is loaded with a load power of 2200 W at t = 1:25*sec* and removed at t = 2:45*sec*. The dynamic performance of the SEIG utilizing IFOC is introduced in Fig. 10. These results confirm good tracking characteristics of the stator currents and DC-link voltage for the CRPWM converter. The load regulation performance for the CRPWM converter is shown in Fig. 11. At t = 1:25*sec*, the CRPWM converter is subjected to a load power of 2200 W. The corresponding q-axis current remained constant due to constant rotor flux orientation. The slip angular frequency also increased due to the increase of the q-axis current. However, the DC-link voltage rejected this disturbance and maintained constant at the reference value. It is clear from these results that good tracking and regulation performance are attainable due to the presence of the IFOC for the SEIG system. The voltage controller provides a rapid and accurate response for the reference. Also, the proposed controller quickly returns the voltage to the reference under full load with a maximum dip of 16 V. It is evident that the proposed control scheme illustrates a satisfactory performance with good tracking characteristics. The resulting regulation performance is also much better. All results obtained confirm the effectiveness of the proposed controllers for an SEIG feeding a CRPWM converter.

9.3 Dynamic Performance of the WECS Connected to the Utility Grid

In order to predict the performance of the proposed SEIGWECS for MPPT, extensive simulation studies are carried out. Simulation waveforms are developed at different wind speeds (5, 8 and 10m/sec) to track the maximum power point of the wind turbine. Fig. 12 illustrates the dynamics response of the IFOC of IG and the DC-link voltage at different wind speeds and

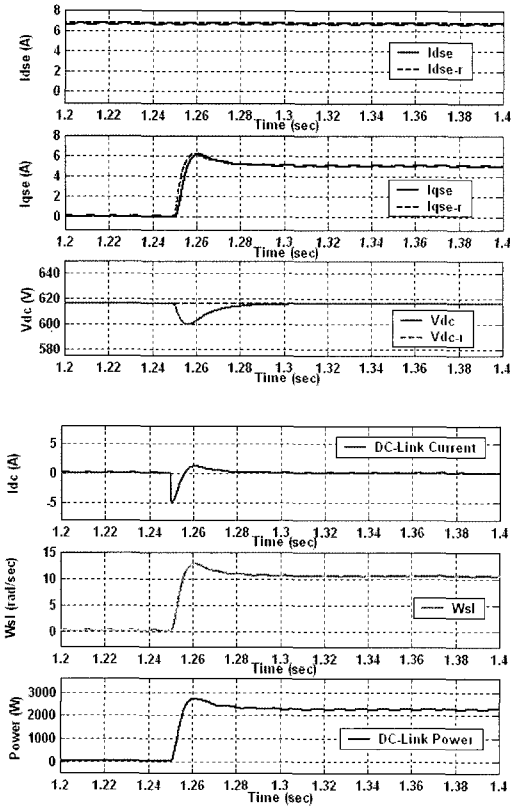

Fig. 11 Disturbance rejection characteristics of the CRPWM converter

maximum power point tracking. The results prove a good dynamic response in tracking the MPP and the regulation performance of the DC-link voltage. The same dynamic response is enlarged in Fig. 13 to show the disturbance rejection performance. At t = 1*sec*, the wind speed was 5 m/sec and the maximum power corresponding to this wind speed about 400 W. The tracking and disturbance rejection performance of the stator currents and DC-link voltage proves a good response and the effectiveness of the proposed controllers. At t = 2*sec*, the wind speed is increased to 8 m/s and the MPP about 1600W. Due to the increased load, the actual values of the stator currents, DC-link voltage and the actual power follow their references as shown in Fig. 13. The wind speed is increased at t = 3*sec* to 10 m/sec. The MPP is about 3200W. The IG is loaded with this maximum power while the converter system's actual variables follow their reference values as shown in Fig. 14. The dynamic response of the CRPWM inverter connected to the grid is

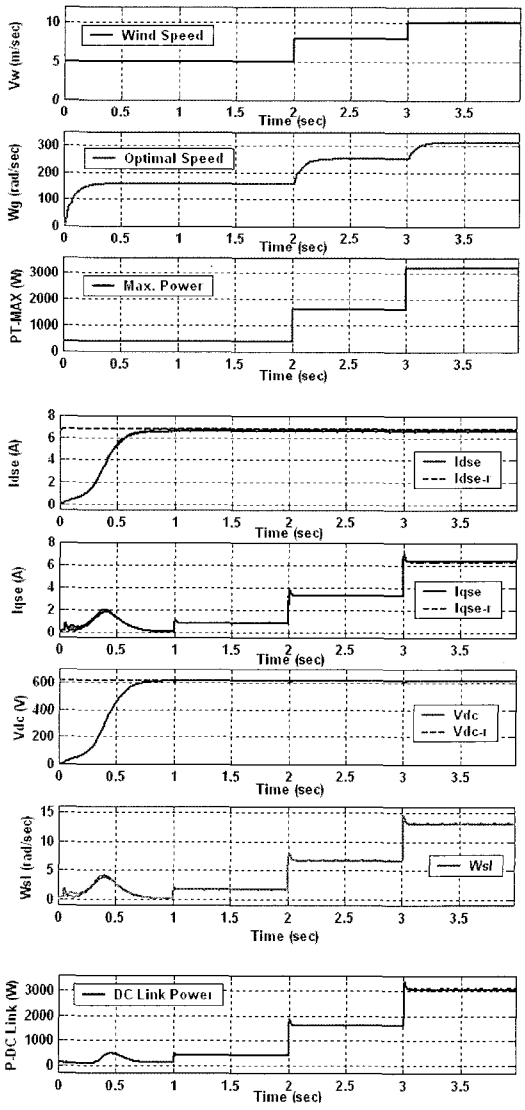

Fig. 12 Dynamic performance of the CRPWM converter with MPPT scheme

given in Fig. 13 at the same wind speed conditions in the MPPT scheme. The current response of the CRPWM inverter in the synchronous reference frame at a wind speed of 5 m/sec is shown in Fig. 14. The results confirm a good tracking performance. When the wind speed is increased to 8 m/sec, the d-q axis currents, active power and reactive power responses are introduced as shown in Fig. 14. The dynamic response in Fig. 15 provides zero reactive power and zero q-axis current which confirms unity power factor operation at different wind speeds. At the same time the d-axis current and the active power follow their references to give the MPPT. The line

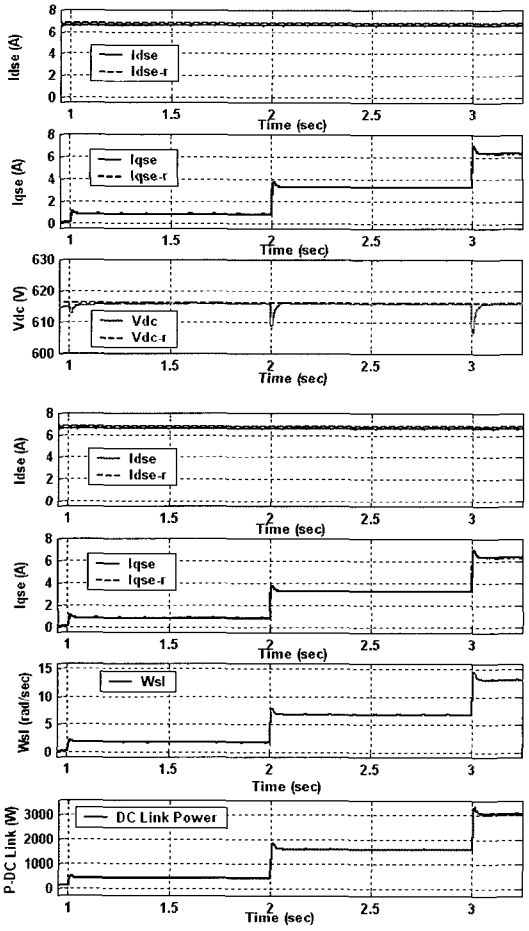

Fig. 13 Tracking and disturbance rejection performance of the CRPWM converter with MPPT scheme

currents at the AC side of the inverter at different wind speeds are shown in Fig. 15. The grid voltage, inverter currents and the injected power to the grid are shown in Fig. 16. From these figures, it is evident that a unity power factor operation is achieved at different wind speeds and loading. It is evident that the proposed control scheme illustrates satisfactory performance and good tracking characteristics. The resulting regulation performance is also much better. All results obtained confirm the effectiveness of the proposed controllers.

10. Conclusion

In this paper, a MPPT control scheme and analytical model are developed to facilitate the systematic design of the integrated wind turbine, SEIG, CRPWM converter, and CRPWM inverter connected to the grid. The dynamic

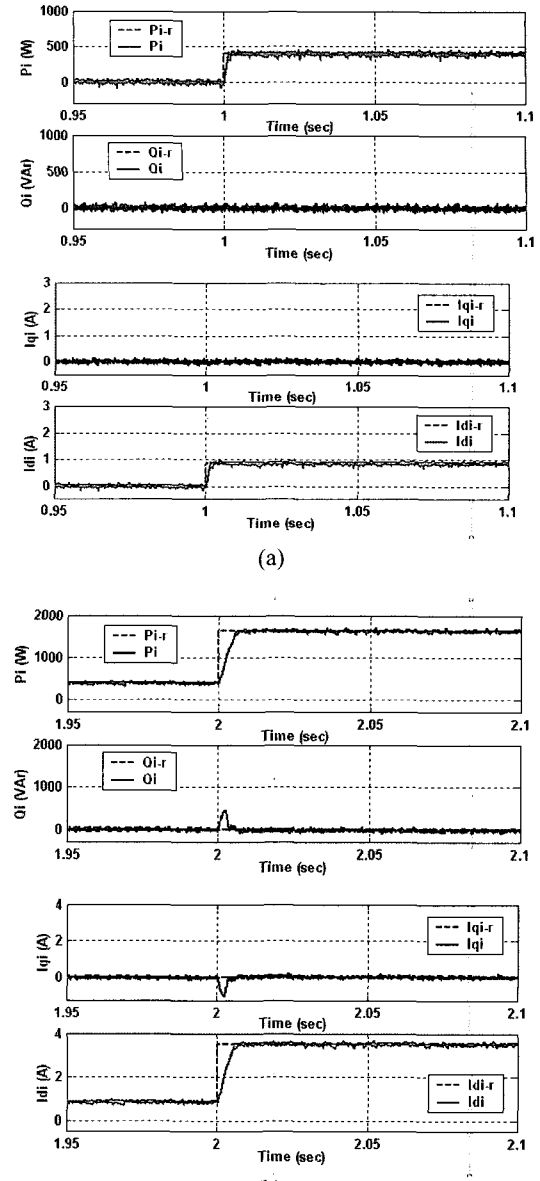

Fig. 14 Dynamic performance of the CRPWM inverter connected to the grid continue (a) Wind speed of 5 m/sec (b) Wind speed of 8 m/sec

performance of the SEIG driven by a wind turbine is accomplished. During voltage build up of the SEIG, variations of the magnetizing inductance are considered. The voltage build up process, DC-link voltage control and current control are accomplished utilizing the IFOC of the SEIG. The rotor flux is aligned to the d-axis in the synchronous reference frame. A voltage decoupler is derived to cancel the coupling terms between the d-q axes. Using an IFOC with rotor flux orientation, the induction

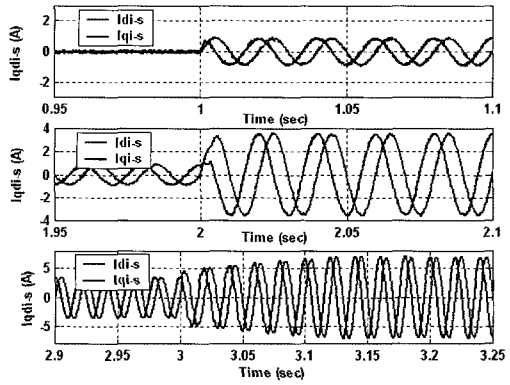

Fig. 15 d-q axes currents of the CRPWM inverter at different v_w

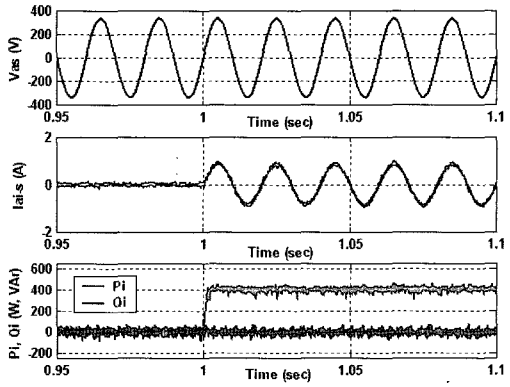

(a)

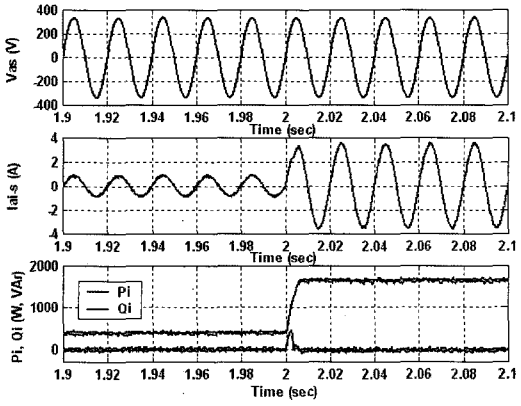

(b)

Fig. 16 Unity power factor operation at different wind speed (a) Wind speed of 5 m/sec (b) Wind speed of 8 m/sec

generator behaves like a separately excited DC generator. The CRPWM voltage source converter regulates the converter DC-link voltage according to a reference value. The converter operates as a boost converter and the voltage regulation is accomplished by controlling the q-axis current of the induction generator. The CRPWM voltage source inverter is designed, according to the VFOC technique, to transfer the maximum power from the wind turbine to SEIG to the grid at a unity power factor. The current controllers are based on the VFOC strategy. While the active and reactive powers are controlled to track the MPPT. Simulation results show the effectiveness of the proposed control techniques used in the CRPWM AC/DC/AC converter/inverter system connected to the grid.

Appendix

Table 1 Table 2

Wind Turbine Parameters		3-phase IG Parameters	
Power	P_m=3.2 kW	P_e=3.6 kW	R_s =1.7Ω
Blade radius	R=2:26m	V=415 V	R_r= 2.7Ω
Speed	ω_r=196 rpm	I=8 A	L_{ls} =11.7mH
Air Density	ρ=2.7 $kg/m3$	Poles=4	L_{lr} =11.7mH
Gear box	3.57	f=50 Hz	L_m =180 mH

References

[1] D. S. Zinger and E. Muljadi, "Annualized wind energy improvement using variable speeds", IEEE Trans. on IA, Vol. 33, No. 6, pp. 1444 –1447, Nov./Dec. 1997.

[2] P. Bauer, S. W. H. de Hann, C. R. Meyl and T. G. pierik, "Evaluation of electrical systems for offshore wind farms", Proc. of IEEE-IAS annual meeting, pp. 1416–1423, 2000.

[3] D. Seyoum, C. Grantham and M. F. Rahman, "The dynamic charteristics of an isolated self-excited induction generator driven by a wind turbine", IEEE Trans. on IA, Vol. 39, No. 4, pp. 936–944, July/Aug. 2003.

[4] M. Orabi and Tamotsu Ninomiya, "Operating performance of induction generator connected to utility grid during grid separation", in Proc. IEEE ISIE Conference, pp. 1315–1320, 2004.

[5] N. H. Malik and A. H. Al-Bahrani, "Influence of the terminal capacitor on the performance of a self-excited induction generator", *in Proc.* , Vol. 137, No. 2, March, pp. 168–173, 1990.

[6] L. Wang and L. Ching-Huei, "A novel analysis on the

performance of an isolated self-excited induction generator", IEEE Trans. on EC, Vol. 12, pp. 109–117, June 1997.

[7] A. K. Al-Jabri and A. I. Alolah, " Limits on the performance of the three phase self-excited induction generator", IEEE Trans. on EC, Vol. 5, pp. 350–356, June 1990.

[8] J. W. Dixon and B. T. Ooi, "Indirect current control of a unity power factor sinusoidal boost type 3-phase rectifier," IEEE Trans. on IE, Vol. 35, pp. 508-515, Nov. 1998.

[9] H. Sugimoto, S. Moritomo and M. Yano, "A high performance control method of a voltage-type PWM converter", *in Proc. IEEE-PESC Conference*, pp. 360–368, 1988.

[10] R. Datta and V. T. Ranganathan, "A method of tracking the peak power points for a variable wind energy conversion system", IEEE Trans. On EC, Vol. 18, No. 1, pp. 163–168, March 2003.

[11] F. Martinez, J. M. Gonzalez, J. A. Vazquez, and L. C. De Lucas, "Sensorless control of a squirrel cage induction generator to track the peak power in a wind turbine", Proc. of IEEE-IECON Conference, pp. 169–174, 2002.

[12] A. B. Raju, K. Chatterjee and B. G. Fernandes, "A simple maximum power point tracker for grid connected variable speed wind energy conversion system with reduced switch count power converter", Proc. of IEEE-PESC Conference, pp. 748–753, 2003.

[13] R. Pena, R. Cardenas, R. Blasco, G. Asher, and J. Clare, "A cage induction generator using back to back PWM converters for variable speed grid wind energy system", Proc. of IEEE-IECON, pp. 1376–1381, 2001.

[14] M. G. Simoes and B. K. Bose, "Design and performance evaluation of a fuzzy-logic-based variable-speed wind generation system", IEEE Trans. on IA, Vol. 33, No. 4, pp. 956–965, July/Aug 1997.

[15] S. Bhowmil, R. Spee and J. H. R. Enslin, "Performance optimization for doubly fed wind power generation systems", IEEE Trans. on IA, Vol. 35, No. 4, pp. 949–958, July/Aug. 1999.

[15] R. Cardenas, R. Pena and G. Asher, "Power smoothing in wind generation systems using a sensorless vector controlled induction machine driving a flywheel", IEEE-Trans. on EC, Vol. 19, No. 1, pp. 206–216, March 2004.

[16] R. Cardenas and R. Pena, "Sensor-less vector control of induction machine for variable-speed wind energy applications", IEEE-Trans. on EC, Vol. 19, No. 1, pp. 196–205, March 2004.

[17] D. Seyoum, M. F. Rahman and C. Grantham, "Terminal volatge control of a wind turbine driven induction geneator using stator oriented field control", Proc. of IEEE-APEC Conference, pp. 846–852, 2003.

Fayez Fahim El-Sousy was born in Gharbia Prefecture, Egypt in 1965. He received his B.Sc. degree in Electrical Power and Machines Engineering from Menoufia University, Egypt in 1988. He received both his M.Sc. degree and his Ph. D degree in Electrical Power and Machines Engineering from Cairo University, Egypt in 1994 and 2000 respectively. Since 1990, he has been with the Department of Power Electronics and Energy Conversion at the Electronics Research Institute (ERI) where he is currently an associate professor. From April 2004 to October 2004, he was a post doctoral visiting researcher at Kyushu University, Graduate School of Information Science and Electrical Engineering, Energy Conversion Laboratory, Japan. His research interests are in the areas of modeling and control of IM, PMSM, LIM and PMLSM drives, intelligent control, optimal control and power electronics. Dr. El-Sousy is currently interested in the robust control of linear motor Maglev drive systems.

Mohamed Orabi was born in Kena, Egypt, in 1974. He received his B.Sc. and M.Sc. degrees in Electrical Engineering from Elminia University, Elminia, Egypt, in 1996 and 2000 respectively. He received his Ph.D degree from Kyushu University, department of Electrical and Electronic Systems Engineering, Japan. Since 1998, he has been associated with the department of Electrical Engineering, Faculty of Engineering in Aswan, South Valley University as an administrator, since 2000 as a research assistant and since 2004 as an assistant professor. His research interests include developing and designing of switched mode power converters and their applications in power factor correction, stability problems, nonlinear phenomena chaos and period doubling bifurcation.

Hatem M. Godah received his M.Sc. and Ph.D from Al Azhar University, Cairo, Egypt in 1996 and 2003 respectively. Since 1991 he has been with the department of Power Electronics & Energy Conversion, Electronics Research Institute (ERI). In 1999, he was a visiting PhD candidate student in the CMD laboratory, POSTECH University, South of Korea. He is currently an assistant professor in ERI. His research interests include digital controller hardware, electric drives and power factor correction.